7

Long-term solar variability: What does theory say?

{ch:long_dyn}

It bears repeating: there currently exist no concensus model for the dynamo process(es) powering the solar magnetic cycle, nor for the magnetic backreaction mechanism(s) regulating its amplitude. This evidently does not augur well for the understanding (and/or prediction) of variations of solar activity on long timescales, which is the focus of this chapter, but we shall proceed nonetheless. "Long timescale" refers here to variations of the cycle amplitude and/or duration unfolding over multi-decadal timescale or more, observational evidence for which having been presented in the preceding chapter. Of particular interest in this context are the Grand Minima episodes of strongly suppressed activity, such as the 1645-1715 Maunder Minimum (REF Fig).

Ref to MM Fig

From the point of view of dynamo modeling, two broad classes of explanations exist for Grand Minima:

- Extreme modulation of the cycle amplitude, with the same dynamo-driven cycle perduring through a Grand Minimum, but at amplitude values too low for sunspot formation.
- Intermittency, meaning a transition between two distinct dynamo states, one being the primary "normal" cycle, and the other not necessarily cyclic but characterized by a magnetic field too weak for sunspot formation.

Extant data, as reviewed in chapter 6, currently does not allow to discriminate unambiguously between these two classes of explanations. The cyclic signal observed in the ^{10}Be record across the Maunder Minimum (Beer et al., 1998, see also §X.Y herein) suggests sustained cyclic activity, as one would expect under a Grand Minimum scenario invoking amplitude modulation. On the other hand, the observed non-periodic recurrence of Grand Minima, as well as their significant variability in duration, is typically easier to produce in intermittency-based scenarios. Part of the difficulty goes

Ref to MM Fig?

back to the ill-understood quantitative link between sunspots and the overall strength of the dynamo-generated internal magnetic field. While the two are clearly correlated (REF previous chapter), the relationship is not linear, and is likely characterized by a threshold at low magnetic field strength.

In this context another dynamo property will play an essential role: whether or not the dynamo is self-excited, i.e., can magnetic field amplification take place from an arbitrarily weak seed field. A dynamo relying on differential rotation shear and the classical turbulent α-effect is in principle self-excited, while a solar cycle model invoking, e.g., the Babcock-Leighton mechanism or flux tube instabilities for poloidal field regeneration is not. In these latter case, if the primary dynamo "turns off" for whatever reason, a distinct inductive mechanism must be invoked to restart it again.

In the remainder of this chapter a survey is presented of the various dynamo-based scenarios put forth as explanatory frameworks for long timescale variations in solar activity, including the occurrence of Grand Minima and Maxima. The various dynamo models reviewed in chapter 5 will serve as starting points towards this program. Nonlinear modulation and the complex interplay of stochastic forcing and nonlinearities leading to intermittency are first explored in §§7.1 and 7.2 using very simple low-order models, after which representative examples occurring in spatially-extended mean-field and mean-field-like dynamo models, as well as global MHD simulations, are reviewed in §7.3. Based on this survey of extant modelling framework, the issue of long-term predictability is revisited in §7.4.

7.1 Nonlinear amplitude modulation {sec:amplmodul}

Parity modulation, energy exchange between flow and field (LOok up Brun paper on this)

Type 1,2: Knobloch example, Tobias 1997

3D Fig ? Ask Steve ?

7.2 Stochastic forcing and nonlinearities {sec:stochforc}

Amplitude modulation driven by stochastic fluctuations of the dynamo number, as illustrated on Fig 5.10, can lead to modulation patterns unfolding on timescales much longer than the coherence time of the fluctuations. Specific examples of this effect in mean-field dynamo models have already been presented on Figure 5.11.

A more extreme form of amplitude variation can occur if stochastic fluctuations push the solution far across the bifurcation point and into the

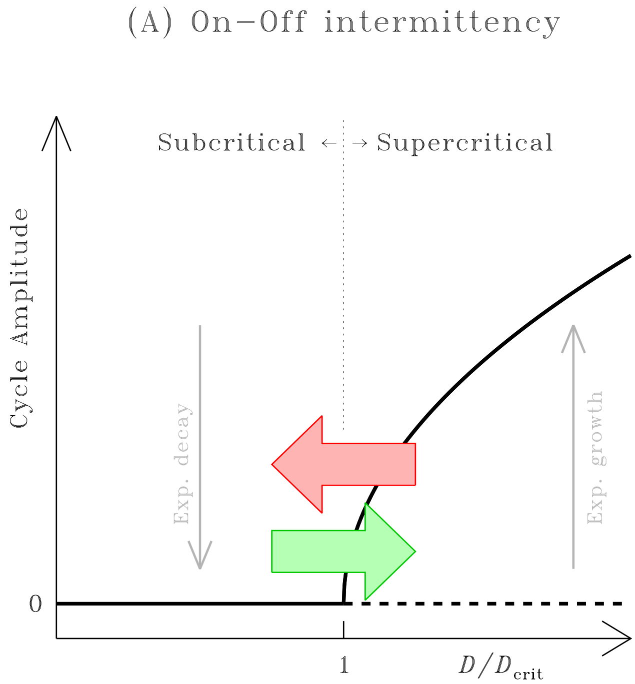

Figure 7.1 On-off of intermittency in a self-excited nonlinear dynamo models without a lower operating threshold on the field strength/cycle amplitude. Stochastic decrease of the dynamo number push the solution into the subcritical regime (red arrow) and later back into the supercritical regime (green arrow) by stochastic increase of the dynamo number. {fig:Hopf2A}

subcritical regime; the cycle amplitude then undergoes exponential decay to the fixed-point trivial solution $\mathbf{B} = 0$, and the dynamo can only restart once a favorable fluctuation pushes the system back into the supercritical regime. This type of behavior, illustrated schematically on Figure 7.1, is known as *on-off intermittency* (Platt et al., 1993). It characterizes self-excited dynamo processes in which amplification remains possible even if the magnetic field falls to very low amplitude, which is the case e.g. for dynamo action driven by the turbulent electromotive force (§3.3.3). Under this scenario the mean duration of quiescent episodes is determined by the decay and growth timescales of the dynamo in the range of dynamo numbers spanned by the fluctuations. This represents an attractively simple explanation for Grand Minima, but is predicated on the dynamo operating relatively close to criticality.

The low-order model of Cameron and Schüssler (2017) introduced in §**??**

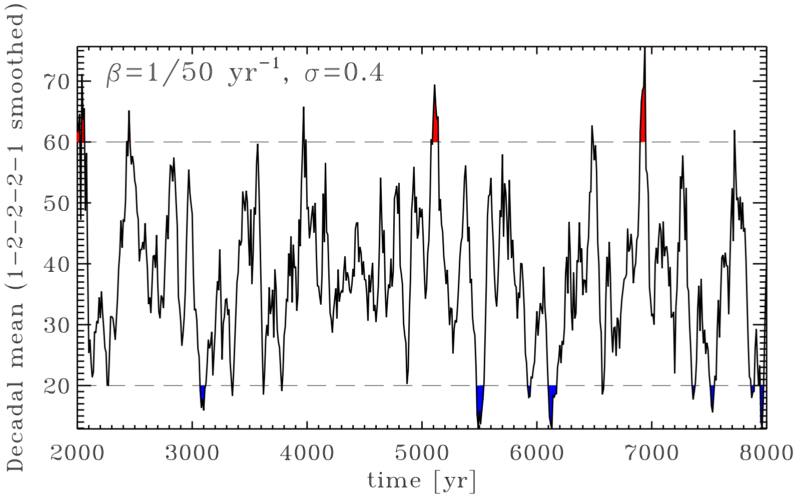

Figure 7.2 Segment of a time series of smoothed decadal mean amplitude (1-2-2-2-1 smoothing window) produced by the Cameron and Schüssler (2017) stochastically forced low-order model, with solar-calibrated parameter values $\beta = 0.02\,\mathrm{yr}^{-1}$ for the linear growth rate, $\sigma = 0.4$ for the stochastic forcing amplitude. The horizontal dashed lines drawn at 20 and 60 indicates the lower and upper thresholds used to identify Grand Minima (colored in blue) and Grand Maxima (red) epochs. Figure produced from numerical data kindky provided by R. Cameron. {fig:cs17intermitt}

offers a particularly simple example of on-off intermittency. Figure 7.2 shows a time series produced using this model. This plot, (and many subsequent similar Figures) has been constructed such as to mimic the radioisotope-based reconstruction of solar activity levels, as presented on Fig. **??**. in §X.Y. A time series of decadal mean values p_n is first constructed from the higher temporal cadence model output, and the resulting time series smoothed using a 1-2-2-2-1 averaging filter:

REF to appropriate §and Fig in previous chapter

$$\bar{p}_n = \frac{1}{8}(p_{n-2} + 2p_{n-1} + 2p_n + 2p_{n+1} + p_{n+2}) \ . \tag{7.1}$$ {eq:12221}

The resulting time series of $\bar{p}$ is plotted as the solid line on Fig. 7.2. It is characterized by substantial fluctuations including occasional excursions at very high and very low amplitude values. Following the procedure introduced in §X.Y, threshold values of 20 and 60 (horizontal dashed lines) are used to delineate epochs of Grand Minima and Maxima in reconstructed activity, as colored in blue and red. For proper choices of model parameters, the frequency distribution of Grand Minima duration and inter-event waiting times constructed from the model output are both approximately exponential, as expected if the trigger is a stationary memoryless random

REF to previous chapter

Another REF to §in previous chapter

process, and generally consistent with the corresponding distributions characterizing reconstructions based on radioisotopes, as discussed in §X.Y (see Cameron and Schüssler, 2017, for further discussion). In this model the average duration of Grand Minima is controlled primarily by the parameter β, setting the linear growth rate of the dynamo. Moreover, in this model, when the dynamo is pushed in the subcritical regime, the solution is still oscillatory even though the amplitude is decreasing exponentially; residual cyclic activity during Grand Minima phases, as suggested by some radioisotope reconstructions, can thus be naturally accounted for. As explicitly demonstrated by Cameron and Schüssler (2017), these dynamical properties carry over to a spatially-extended 2-layer Babcock-Leighton model, supporting the claim that thesr results are robust. The source of fluctuations, as captured by the parameter σ, is ascribed to the strong scatter in the E-W tilt of bipolar active regions (see §5.4.3, and §7.3.2 further below).

The low-order model of Passos et al. (2012) introduced in §5.3.7 also exhibits on-off intermittency when subjected to stochastic forcing. The dynamical behavior is now more complex (as per Fig. 5.8) but the intermittency mechanism is still basically that illustrated on Fig. 7.1. Passos et al. (2012) impose uniformly distributed zero-mean forced fluctuations in the numerical parameter a controlling the magnitude of the magnetic backreaction on the meridional flow variable v_p. This introduces variability in the time rate of change of the flow, which directly carries over to the magnetic flux transport terms (first terms on the RHS of eqs. (5.28)–(5.29)). For an unfavorable sequence of fluctuations, the dynamo can be short-circuited and pushed into the subcritical regime. One such event is illustrated on Figure 7.3. The top panel shows time series segments of the three dynamical variables A, B and v (see eqs. (5.28)–(5.30)) including a Grand Minimum, and the bottom panel the corresponding phase space trajectory across that Grand Minimum. On the latter, the black dashed line shows the limit cycle in the absence of stochastic forcing, the gray dots the blurring of this limit cycle when noise is introduced. The colored trajectory shows the impact of a large fluctuations triggering a high amplitude outward excursion in parameter space (blue), with subsequent collapse to the $A = B = 0$ axis (cyan to green). Following recovery of the meridional flow variable, the dynamo grows again as at outward spiralling trajectory (yellow to red).

Under this scenario entry into a Grand Minimum is swift, while recovery to normal cycle behavior is more gradual. The strong increase in magnetic and velocity amplitudes is here a good precursor to the onset of Grand Minima, which recur aperiodically in this model. The frequency distributions of

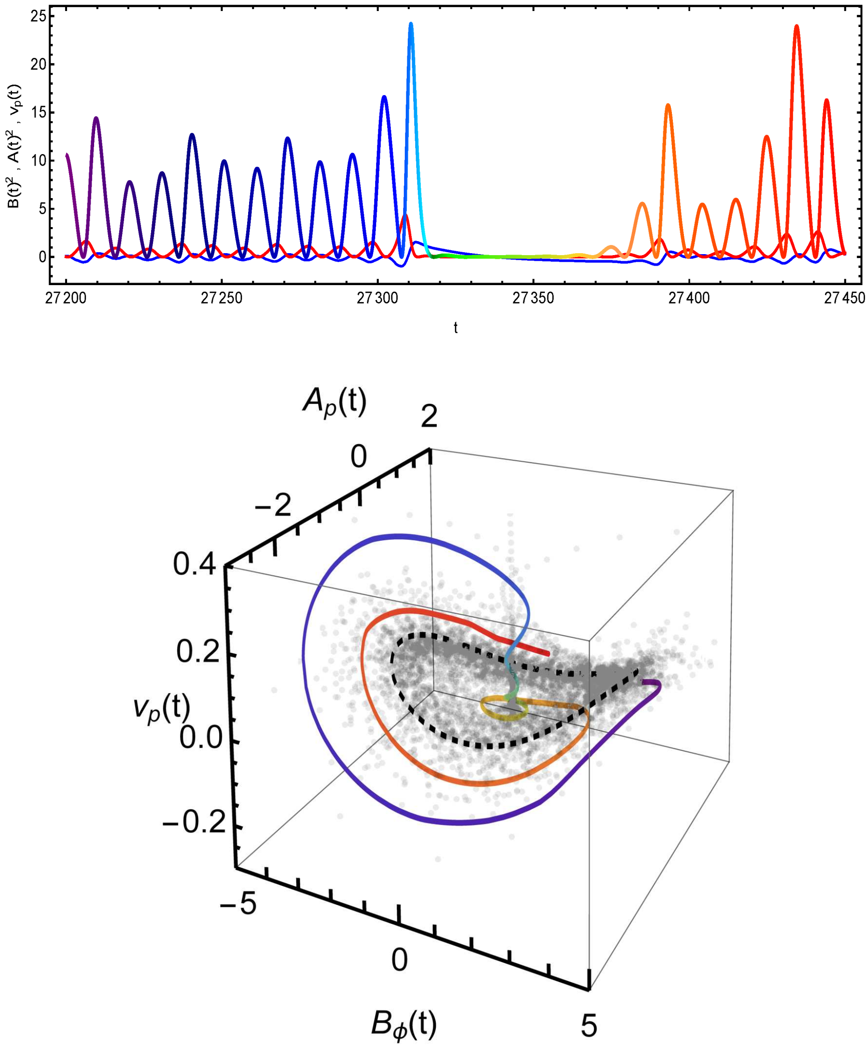

Figure 7.3 A Grand Minimum in the non-kinematic low-order dynamical model of Passos et al. (2012). The upper panel displays time series of the three dynamical variables A (poloidal field amplitude, red), B (toroidal field amplitude, purple to red), and v (meridional flow amplitude, blue) across a Grand Minimum. The bottom panel shows the same Grand Minimum, this time in the form of a phase space trajectory (see text). Adapted from Figs 8 and 11 in Passos et al. (2012).

{fig:BLMaunder}

Grand Minima durations and inter-event waiting times are both approximately exponential, again consistent with a memoryless stochastic trigger.

A distinct form of intermittency can materialize in dynamos that are not

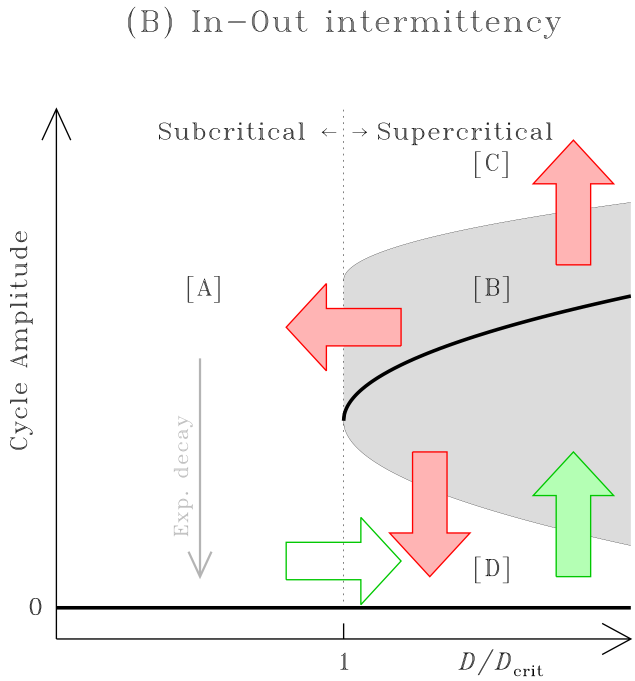

Figure 7.4 In-out intermittency in nonlinear dynamo models subjected to both upper and lower operating threshold on the field strength/cycle amplitude. The limit cycle solution (thick solid line) has a finite-sized basin of attraction, shaded in gray and labeled [B]. Here the trivial $\mathbf{B}=0$ fixed-point solution remains accessible in the supercritical regime, with a basin of attraction corresponding to regions [C] and [D]. Intermittent behavior can now be triggered by stochastic fluctuations either of the dynamo number (horizontal arrow), or of the cycle amplitude itself (vertical arrows). {fig:Hopf2B}

self-excited, due to magnetic field regeneration being subjected to a lower operating threshold. Figure 7.4 illustrates schematically this more complicated dynamical situation. As on Fig. 7.1, the transition from the fixed-point $\mathbf{B}=0$ solution to a cyclic (limit cycle) state occurs when the dynamo number D exceeds its critical value $D_{\rm crit}$. Here, however, at the bifurcation point the limit cycle appears with a finite amplitude, and is characterized by a finite basin of attraction (gray shading). Any initial condition within the gray-shaded area converges to the limit cycle solution (curved thick solid line), while initial solutions starting above or below converge to the $\mathbf{B}=0$ fixed point. This dynamical behavior characterizes dynamo models in which source terms are subjected to a lower operating threshold on the magnetic field; Babcock-Leighton-type models (3.3.6) belong to this variety, since sunspot emergences requires a minimal strength for the participating magnetic flux ropes. In the absence of active region emergences, the regeneration of the poloidal magnetic component cannot take place, and sustained dynamo action is impossible. For specific examples of such a Babcock-Leighton models with lower operating thresholds, see Charbonneau et al. (2005); **?**, as well as Fig. 5.9 herein. Likewise dynamos driven by instabilities of magnetic flux tubes (§3.3.7) also require a minimal field strength for the instability to be excited. In either cases, intermittency can now occur if some internal mechanism manages to knock the cyclic solution out of its basin of attraction.

Stochastic noise could affect the operation of such a dynamo in at least two distinct ways. If the dynamo operates close to criticality, then as with the simpler case depicted on Fig. 7.1 a fluctuation in the dynamo number can push the solution into the subcritical regime (horizontal solid red arrow on Fig. 7.4), following which the cycle amplitude will decay. Unlike for the simpler bifurcation case illustrated Fig. 7.1, here a subsequent stochastic increase of the dynamo number (open green arrow) would push the solution into region [D], which is part of the attraction basis for the $\mathbf{B} = 0$ solution. Restart is then only possible if another source of magnetic field pushes the solution back inside the attraction basin of the cyclic solution (upward-pointing solid green arrow).

In addition, fluctuations in the cycle amplitude (of whatever origin), can push the dynamo outside of the attraction basin of the cyclic solution (vertical red arrows) even if the dynamo number remains in the supercritical regime. The magnitude of the needed fluctuations depend on the details of the dynamo model and amplitude-limiting nonlinearity considered. Note however that even very low noise level can do the trick if the dynamo operates in a regime where the solution wanders close to boundary of the attraction basin, which can happen in the chaotic regimes often accessible to strongly supercritical dynamo solutions. The mean duration of quiescent episodes under this dynamical regime is now harder quantify; as for the simpler on-off intermittency mechanism depicted on Fig. 7.1, it is controlled by the decay and growth timescales of the primary dynamo in regions [A] and [B] on Fig. 7.4, but also by the timescale(s) associated with the secondary mechanism pushing the solution back into the attraction basin ([D]$\to$[B]).

The iterative map considered in §5.3.10 offers a particularly simple example of in-out intermittency. As the solution is pushed far into the supercritial regime, a series of period-doubling bifurcations lead to chaotic modulation, and farther in this chaotic supercritical regime the aperiodically varying amplitude iterate wanders close to the boundary of the attraction basin (see

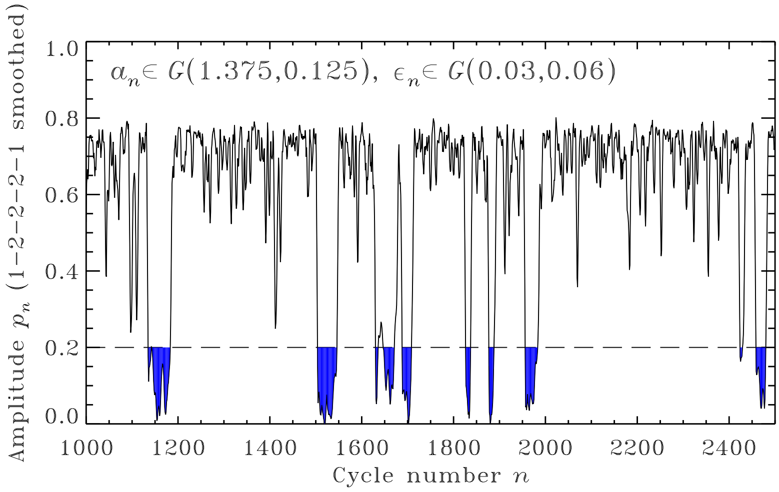

{fig:stochmap} Figure 7.5 Segment of a time series of smoothed cycle amplitude (1-2-2-2-1 smoothing window) produced by the stochastically forced iterative map (7.2). The horizontal dashed line drawn at $p_n = 0.2$ indicates the lower threshold to identify "quiescent" from "active" epochs (see text), the former being colored in blue.

Fig. 5.9A). Once in the chaotic regime, even low amplitude noise, meaning here noise amplitude much smaller than the amplitude iterate, can then trigger intermittency through the [B]→[C] or [B]→[D] routes on Fig. 7.4.

Figure 7.5 shows a representative time series of cycle amplitude p_n, for a stochastically-forced version of this iterative map:

{eq:stochmap}
$$p_{n+1} = 4\,a_n p_n^2(1-p_n) + \varepsilon_n \qquad n = 0,1,2,... \tag{7.2}$$

with

{eq:stochmap2}
$$a_n \in G(1.375, 0.125)\ , \qquad \varepsilon_n \in G(0.03, 0.06)\ , \tag{7.3}$$

where the random deviates a_n and ε_n are extracted anew at each iterations from Gaussian distributions $G(\mu,\sigma)$ of mean μ and standard deviation σ, as indicated. Note that with these choices, a_n is very nearly always in the supercritical regime (cf. Fig. 5.9A), so the [B]→[A]→[B] channel to intermittency is essentially inactive here. In this modified form, the map parameter a_n is now subjected to stochastic fluctuations (multiplicative noise), as introduced in §5.4.1, as well as additive stochastic noise ε_n, representing the action of an additional inductive mechanism, for example a small-scale dynamo. The combined action of these two sources of stochastic forcing causes the solution to move in and out of the attraction basin of the cyclic solution, producing quiescent phases of suppressed cycle amplitude interspersed within epochs of "normal" cyclic behavior, albeit characterized by significant cycle-to-cycle variations in amplitude. Here the system is deemed to have entered a quiescent phase when the amplitude iterate falls below $p_n = 0.2$, which corresponds to the lowest extent of the attraction basin for the deterministic version of this map (see Fig. 5.9). Note how the quiescent phases, colored in blue, have varying durations and show no hint of periodicity on their occurrence. Unlike on the time series of Fig. 7.2, here there are no upward excursion in cycle amplitude in the active mode of operation of the dynamo, i.e., there are no equivalents to Grand Maxima in this very simple model.

This system is characterized by an *intermittency threshold*, namely a minimal additive noise level (upper bound value on ε_n in eq. (7.3)) below which the amplitude iterate cannot climb back into the attraction basis of the limit cycle. Sufficiently far from this threshold, and provided the ε_n remain significantly smaller than the cycle amplitude p_n, the frequency distribution for the durations of quiescent phases shows little dependence on the additive noise level, except in the tail of very long duration quiescent phases. Likewise, the distribution for active phase durations is exponential and largely insensitive to the additive noise level, even though low-level noise is essential to this intermittency mechanism (see Charbonneau, 2001, 2005, for further details and illustrative examples).

7.3 Case studies {sec:cases}

It is not *a priori* obvious that the production of Grand Minima and other long timescale behaviors in the various highly simplified "toy models" considered above necessarily carries over to more realistic spatially-extended solar cycle models including solar-like large-scale flows and spatially-varying inductive mechanisms. In this section we consider in some detail a few "case studies", i.e., representative instances of such models in which counterparts to these long timescale modulation patterns and intermittent behaviors are indeed observed. Many more such examples can be found in the published literature; the selection that follows is meant primarily to illustrate the wide range of possible Grand Minima scenarios.

7.3.1 Self-excited kinematic dynamos: fluctuating α-effect {ssec:alphafluct

Many extant mean-field solar cycle models achieve the production of long timescale modulation, including Grand Minima and Maxima, through forced stochastic fluctuations of the dynamo source terms. The most straightforward avenue is on-off intermittency in mildly supercritical models, as illustrated schematically on Fig. 7.1 and captured quantitatively in the low-order dynamical system model of Cameron and Schüssler (2017) described in the preceding section.

Our first case study is an example of this intermittency mechanism occuring in a stochastically-forced version of the mean-field dynamo model of Kitchatinov and Olemskoy (2012). This 2D kinematic axisymmetric mean field-like model solves dynamo equations equivalent to the $\alpha\Omega$ version of eqs. (5.10)–(5.13), with a non-local surface source term capturing the regeneration of the large-scale poloidal magnetic component through the Babcock-Leighton mechanism. The model also incorporates a solar-like internal differential rotation profile and single-cell meridional flow, similar to those introduced for model BLMC in §5.2.2, but operates at low magnetic Reynolds number $\mathrm{Rm} = 10$, so that the transport of magnetic flux takes place in the diffusion-dominated regime. This dynamo is self-excited, as it does not incorporate a lower magnetic field strength threshold on its poloidal source term.

The stochastically-forced version of this model, described in Olemskoy and Kitchatinov (2013), introduces fluctuations in the surface poloidal source term that depend on both space and time, a setup far more realistic physically that the simpler and more commonly adopted forced fluctuation of just the dynamo number. In keeping with the idea that their poloidal source term models the Babcock-Leighton mechanism of poloidal field regeneration through active region decay, Olemskoy and Kitchatinov (2013) set the coherence length and time of their forcing function at 6° and one month, typical values for the latitudinal extent and lifetime of a large active region (see their §2.3 for a full description of their forcing formalism).

Figure 7.6 shows some sample results generated with this dynamo model. The top panel shows a time-latitude diagram of the deep toroidal magnetic field, the model's equivalent to the sunspot butterfly-diagram, and the bottom panel a 1-2-2-2-1 smoothed time series of peak integrated magnetic flux, linearly scaled to yield sunspot number-like numerical values. The model is run here in the mildly supercritical regime, so that the triggering of Grand Minima takes place through on-off intermittency (Fig. 7.1), but with an interesting new twist. The latitudinal dependence of stochastic forcing leads to the excitation of higher-order dynamo modes, which can strongly interfere with the operation of the fundamental dynamo mode even if the latter remains supercritical from the point of view of the net dynamo number (on this point see also Hoyng et al., 1994; Ossendrijver et al., 1996). This shows up prominently on the time-latitude diagram of Fig. 7.6, as a strong

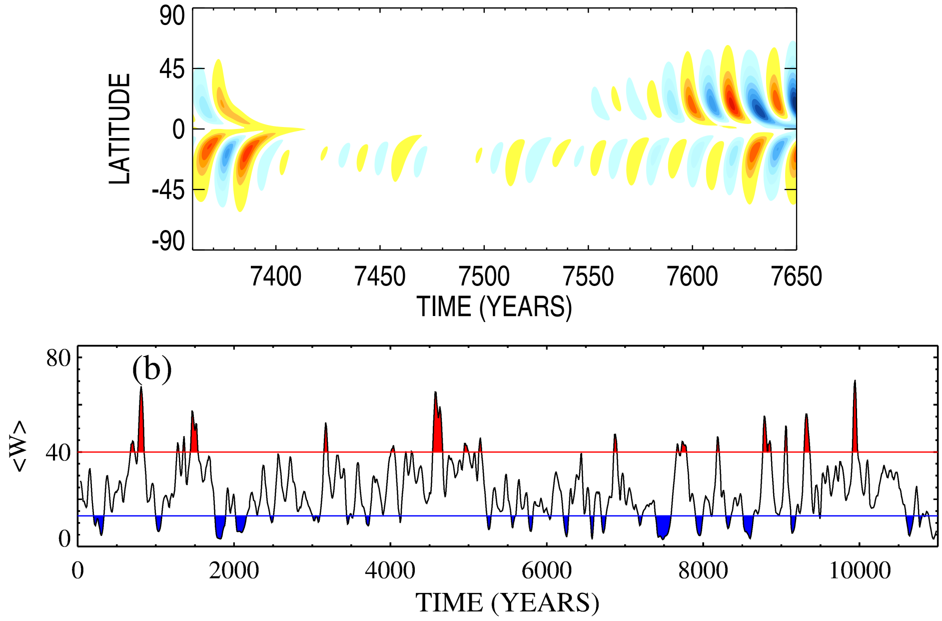

{fig:KitchOlem1} Figure 7.6 Grand Minima in the stochastically-forced Babcock-Leighton solar cycle model of Olemskoy and Kitchatinov (2013). The top panel is a time-latitude diagram of the toroidal magnetic component, akin to the sunspot butterfly diagram in this model. The bottom panel shows the 1-2-2-2-1 smoothed time series of cycle amplitudes, in a format similar to Figs. 7.2 and 7.5. The threshold values for Grand Maxima (red) and Minima (blue) are set at values that match the fraction of time spent in these phases, as inferred from cosmogenic radioisotope-based reconstructions. Graphics kindly provided by L. Kitchatinov.

hemispheric asymetry in activity level, persisting here from the onset to the recovery phase of this model Grand Minimum. Note also the residual cyclic activity throughout the Grand Minimum, here restricted to the Southern hemisphere.

Interestingly, the frequency distribution of Grand Minima durations, as reconstructed from the bottom panel of Figure 7.6, shows a hint of bimodality akin to that characterizing some radioisotope reconstructions. As with the simple low-order model of Cameron and Schüssler (2007), the mean duration of Grand Minima is primarily set by the linear growth rate of the dynamo, and a solar-like distribution results from operating the model in the mildly supercritical regime. The inter-event waiting time distribution is again approximately exponential, as expected from a stationary memoryless random process. REF to appropriate Fig in previous chapter

For other examples of intermittency through stochastic forcing of a self-excited dynamo, see also Ossendrijver et al. (1996); Tworkowski et al. (1998); Moss et al. (2008); Usoskin et al. (2009).

{ssec:2alphafluct}

7.3.2 Non-self-excited dynamos: dual source terms

In dynamo models that are not self-excited, recovery from a Grand Minimum may require a second inductive mechanism to push the primary dynamo back above its operating threshold (upward-pointing green arrow on Fig. 7.4). Our next case study offers an example of such a dual-dynamo solar cycle model.

The kinematic 2D mean-field-like model of Passos et al. (2014) invokes the Babcock-Leighton mechanism of poloidal field regeneration for its primary dynamo, and uses a solar-like differential rotation and a quadrupolar meridional flow (single cell per meridional quadrant), as described in Chatterjee et al. (2004). In the Passos et al. (2014) implementation, the Babcock-Leighton mechanism operates in a finite range of toroidal field strengths $10^3 \leq B_\phi \leq 10^5$ G; its dynamical behavior is thus akin to Fig. 7.4, i.e., the dynamo has a finite basin of attraction in the supercritical regime. To allow restart of the primary dynamo, a secondary dynamo relying on the turbulent electromotive force associated with convection is added within the bulk of the convection, quenching at a field strengh $B_\phi > 10^4$ G (on such "dual-dynamos", see also Dikpati and Gilman, 2001; Mason et al., 2002; **?**). Forced stochatic fluctuations are imposed on either or both of the two dynamo numbers controlling the strength of the poloidal field regenerative terms, i.e., the stochastic driver affects only the $T \to P$ portion of the dynamo loop. The onset and recovery from a Grand Minima thus follows the [B]→[A]→[D]→[B] path on Fig. 7.4.

Figure 7.7 depicts a typical Grand Minimum arising in this dual-dynamo model. The top panel is a time-latitude diagram of locations of bipolar magnetic region emergences, and the bottom panel shows the corresponding time-latitude diagram for the deep-seated toroidal magnetic field generating these emergences. Note how strong hemispheric asymetries and residual cyclic activity is observed across the Grand Minima, analogous to the Maunder Minimum.

Ref to MM §

The magnitude and partial overlap in the operating range of the two dynamo source terms is important and requires some fine tuning for the desired behavior to materialize. The basic (non-fluctuating model) introduces a turbulent α-effect of a magnitude low enough to cause minimal changes in the magnetic cycles generated by the Babcock-Leighton source term in its absence. The frequency and mean duration of Grand Minima episodes is found to depend on the magnitude and fluctuation levels of both

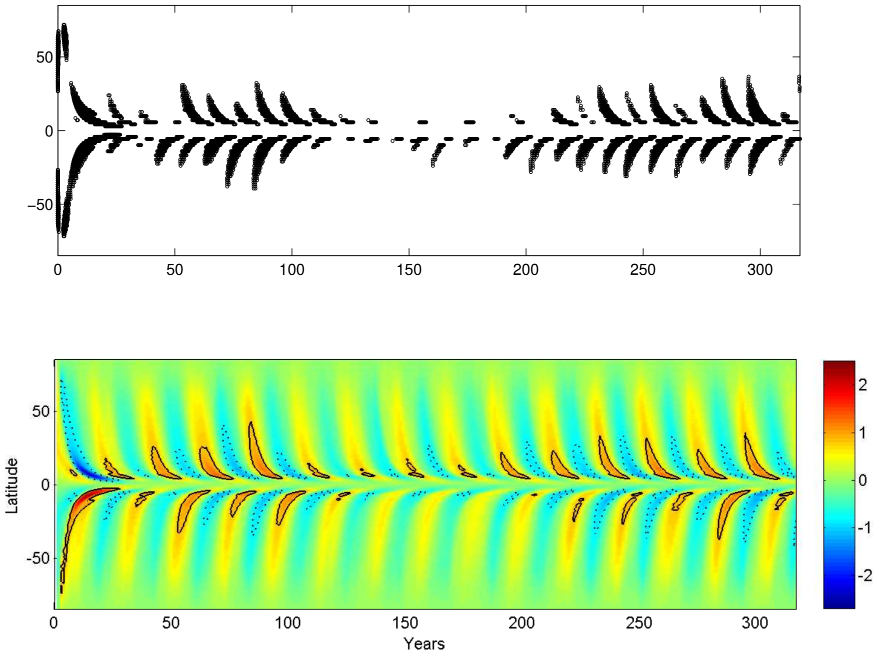

Figure 7.7 A Grand Minimum in the stochastically-forced dual-dynamo model of Passos et al. (2014), a 2D axisymmetric kinematic mean-field-like dynamo combining a Babcock-Leighton surface poloidalsource term and a classical α-effect distributed in the convection zone. Time-latitude diagrams of bipolar magnetic region emergences (top panel) and deep-seated toroidal magnetic field (bottom panel) are shown, spanning a Grand Minimum episode. The first 30 simulated years are still relaxing the (arbitrary) initial condition.

{fig:GMPassos14}

of these poloidal source terms. A supercritical Babcock-Leighton dynamo and strongly fluctuating mean-field α-effect leads to long Grand Minima, while a mildly critical Babcock-Leighton dynamo and smaller fluctuations in the mean-field α-effect yields shorter and more frequent Grand Minima. In all cases the occurrence of Grand Minima is aperiodic, as expected from a stochastic trigger.

For the solution displayed on Figure 7.7, this dual-dynamo system never entirely shuts off, as evidenced by the sustained regular polarity reversals of the deep toroidal field (bottom panel). The turbulent α-effect is preventing the primary dynamo from becoming strongly subcritical, maintaining it instead close to criticality. Grand Minima in this model are perhaps better characterized as being caused by a form of self-regulating amplitude modulation combined with a threshold effect, rather than true intermittency.

In solar cycle models relying on the Babcock-Leighton mechanism of polar field reversal and regeneration, the variability in the emergence rates and physical properties of bipolar active regions amounts to a source of strong stochasticity in the $T \to P$ segment of the dynamo loop. Figure 5.12 already demonstrates that a single active region with extreme characteristics (such as a large magnetic flux and tilt angle departing strongly departing from Joys's law) can strongly alter the buildup of the surface dipole, and consequently the amplitude of the subsequent magnetic cycle cycle. Such occurrences have been observed on the sun (Cameron et al., 2014), and are oven invoked as the physical origin of the strong stochasticity introduced in an ad hoc manner in many extant Babcock-Leighton solar cycle models of varying levels of complexity. The models of Cameron and Schüssler 2017, Olemskoy and Kitchatinov 2013 and Passos et al. 2014, just considered above, are all cases in point.

Our next case study builds on the 2×2D solar cycle model ofLemerle and Charbonneau (2017) described in §5.4.3. This kinematic dynamo model incorporates a detailed description of surface flux evolution and bipolar magnetic flux emergence and surface flux evolution, the the physical characteristics of the later being drawn from statistical distributions built from observed solar active regions. In some rare and extreme cases, the negative impact of a large, "rogue" bipolar active region on the global dipole can be strong enough to shift the phase relationship between the surface dipole and internal magnetic field to the point of derailing the cycle and effectively pushing the model into the subcritical regime ([B]→[A] red arrow on Fig. 7.4; see §X.Y in Nagy et al. 2017 for a specific example).

As with the simpler mean-field-like model of Passos et al. (2014), once the dynamo shuts off and enters a Grand Minimum, a secondary dynamo process is required to kickstart it again for recovery to normal cyclic behavior. Once again a weak mean-field α-effect can achieve the desired effect. Under "normal" conditions the magnetic field generated by the (primary) Babcock-Leighton dynamo quenches the α-effect of the (secondary) turbulent dynamo. But once the primary dynamo shuts off, the magnetic field decays under the operating threshold of the turbulent α-effect, which then turns on and pushes the magnetic field back above the operating threshold of the primary dynamo, and normal cyclic behavior resumes; as with the Passos et al. (2014) model just considered, relatively fine tuning of the magnitude and quenching levels of the two source terms is required to obtain the desired behavior.

Figure 7.8 A Grand Minimum in the Lemerle and Charbonneau (2017) Babcock-Leighton dynamo model including a secondary turbulent α-effect concentrated at the bottom of the convection zone. The top panel is a time-latitude diagram of the surface radial field, while the bottom time-latitude diagram displays the surface density of emerging bipolar magnetic regions. Simulation and graphics courtesy of D. Ölçek.

{fig:GMDeniz}

Figure 7.8 displays a representative Grand Minimum occurring in this model, in the form of surface time-latitude diagrams of the surface radial field component (top) and density of emerging bipolar magnetic regions (bottom).

occasional BMR emergences (failed restarts) but no clear periodicity across GM

strong hemispheric asymetry entering and exiting GM hemispheric asymetry as precursor signal ?

Figure 7.9 shows a time series of smoothed cycle amplitudes for the same model run as on Fig. 7.8, but over a 10^4 yr time span, in the now usual format. Grand Minima and Maxima recur aperiodically, and with former showing a much wider range of durations than the latter. Here once again the onset of Grand Minima and Maxima is driven by memoryless stochastic process, leading in both cases to inter-event waiting time distributions that

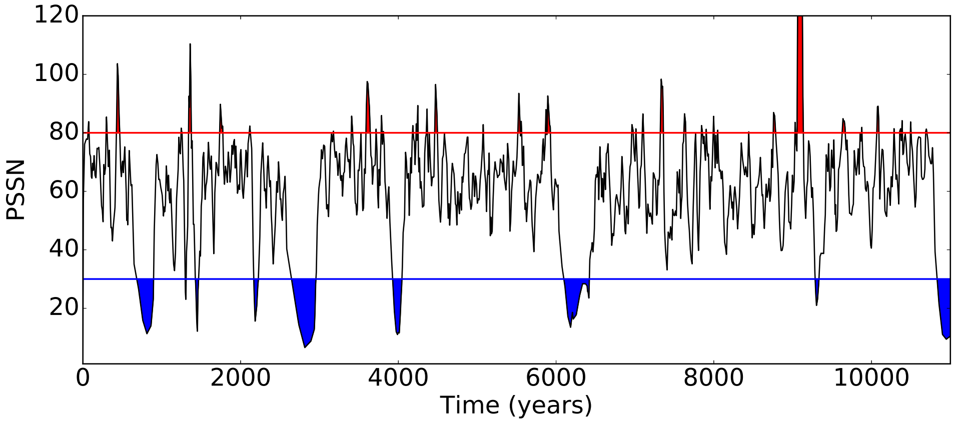

Figure 7.9 Time series of 1-2-2-2-1 smoothed cycle amplitudes in an extended simulation run of the Lemerle and Charbonneau (2017) Babcock-Leighton dynamo model including a secondary turbulent α-effect. As in earlier such Figures Grand Maxima and Minima are colored in red and blue respectively. The threshold value used to identified the latter is chosen so as to reproduced cosmogenic radioisotope-based estimates for the fractional time spend in Grand Minima states. Note the extreme Grand Maximum at $t \simeq 9100$ yr. Simulation and graphics courtesy of D. Ölçek. {fig:GMDenizts}

are exponential in form. The duration of Grand Minima is set by two factors: the decay time of the residual large-scale magnetic field once the dynamo shuts off determines at which point quenching of the α-effect will vanish; and the growth time of the associated $\alpha\Omega$ dynamo process. For the solutions displayed on Fig. 7.8, the former dominates and effectively sets the mean duration of Grand Minima phases. Their wide range of durations ultimately reflects the state of the internal field at the time the primary Babcock-Leighton dynamo shuts off.

For other examples of in-out intermittency in non-self-excited dynamos through the interplay of dual magnetic induction mechanisms, see Schmitt et al. (1996); Ossendrijver (2000b); Charbonneau et al. (2004); Karak and Choudhuri (2013); Hazra et al. (2014a).

{ssec:cmfluct}

7.3.3 FLuctuating meridional flow

FTD: transport between source regions essential; if short-circuited, dynamo dies.

Karak, Choudhuri & co

7.3.4 self-excited dynamos: nonlinear magnetic backreaction on differential rotation

In all of the above case studies, cycle fluctuations are generated in the $P \to T$ segment of the dynamo loop. We now turn to the $T \to P$ segment, specifically the nonlinear magnetic backreaction on differential rotation. As discussed already in **??**, this mechanism can achieve saturation of the dynamo at fixed cycle amplitude; however, in the low Prandtl number regime, it can also generate extreme amplitude modulation which, in conjunction with a field strengh threshold on sunspot formation, can offer a viable physical explanation for Grand Minima and Maxima.

Our first case study in this family is the dynamo model described in Bushby (2006). This is a non-kinematic but otherwise conventional self-excited 2D axisymmetric $\alpha\Omega$ dynamo model, relying on differential rotation shear and the turbulent α-effect as inductive mechanisms. The model uses a solar-like internal differential rotation profile, a negative (N-hemisphere) α-effect concentrated at low latitudes, and a magnetic diffusivity dropping rapidly below the convection zone, yielding an interface-like dynamo. The nonlinear backreaction on differential rotation uses the strategy outlined in §5.3.6, namely solving only for the variations of the differential rotation with respect to an imposed solar-like profile (viz. eq. (5.26)), via the solution of a reduced dynamical essentially identical to eq. (5.27.

Figure 7.10 shows a set of magnetic energy time series generated using this model, obtained for various combinations of dynamo and Prandtl numbers, as labeled. Recall (from §5.3.6) that the latter sets the timescale over which magnetically-induced variations of large-scale flows are attenuated. At low dynamo number D and Prandtl number $\mathrm{Pm} \sim 1$, the dynamo develops a constant-amplitude cycle (not shown), here with a period $P \simeq 10^{-2}\tau$, where τ is the magnetic diffusion time (viz. eq. (3.9)). This primary cycle remains in in the low-Pm regime, but there now also appears a modulation on a timescale much longer than the primary cycle, with period given approximately by P/Pm (panel A). This modulation becomes chaotic as the dynamo is pushed farther into the supercritical regime (panel B). At fixed dynamo number, the modulation period increases as Pm decreases (cf. panels C and D). Parity (red) modulation also occurs in all solutions, becoming quite irregular in the more supercritical solutions and/or at low Prandtl numbers. without any preferred symmetry emerging. Careful comparison of the black and blue time series on Fig. 7.10 reveals that the kinetic energy associated with the flow perturbation lags temporally the magnetic energy. While the overall amplitude of differential rotation variations increases with

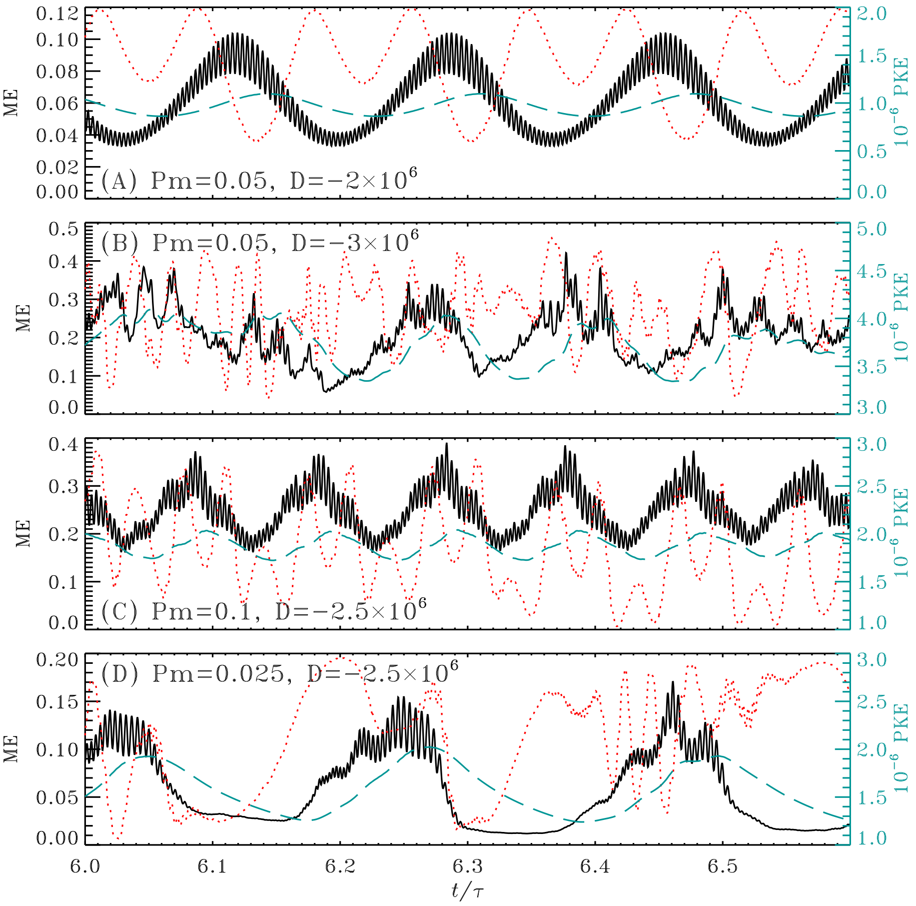

Figure 7.10 Cycle amplitude modulation in the non-kinematic $\alpha\Omega$ mean field model of Bushby (2006). The four panels show time series of magnetic energy (ME, in black), perturbation kinetic energy (PKE, in blue-dashed) and parity (red-dotted, scaled from $[-1, 1]$ to the vertical extent of each plot), for different combinations of dynamo and Prandtl numbers, as labeled. Time is in unit of the magnetic diffusion time, and the critical dynamo number for the range of model parameter values explored is $\simeq -1.5 \times 10^6$ for Pm ~ 1. Plotted from numerical data kindly provided by P. Bushby. {fig:nkin1}

decreasing Prandtl number on long timescales, the amplitude of torsional oscillations on the timescale of the primary cycle vary proportionally with Pm. Refering back to the simple low-order order model of §7.1, these non-kinematic solutions typically exhibit concurrently both Type I and Type II patterns of amplitude modulation.

For the strongly modulated solution of Fig. 7.10D, it is tempting to identify the modulation phases of very low magnetic energy (ME$\leq$ 0.05 say) with Grand Minima. Entry and exit from these Grand Minima is gradual and often accompanied by strong hemipheric asymetry, a natural consequence of parity modulation. Although not obvious on Fig. 7.10D, the primary cycle does perdure through Grand Minima, albeit at very low amplitude. In this parameter regime Grand Minima tend to recur quasi-periodically, on a timescale inversely proportional to the Prandtl number, their roughly constant duration being set by the time required to dissipate the flow variations induced by the Lorentz force.

In the strongly chaotic solution of Fig. 7.10B it is also certainly possible to identify phases of very low magnetic energy with Grand Minima. They are now markedly aperiodic and not as well delineated as for the solution plotted on panel D. This solution also exhibits, on very long timescales, an additional modulation pattern whereby both magnetic and perturbation kinetic energy undergo a rapid upwards excursion by over two orders of magnitude, followed by slower recovery to the "basal" chaotic state. This could be interpreted as Grand Maxima in this dynamo model. In all these solutions, introduction of α-quenching as an additional amplitude-limiting regularity tends to stabilize the modulation patterns, in both magnetic energy and parity.

Figure 7.11 shows the behavior of a similar non-kinematic 2D axisymmetric dynamo model, this time using a full α-tensor extracted from the global MHD "millenium" simulation discussed in §**??** (see in particular Fig. 5.4). The top panel shows time series of magnetic energy (black) and parity (red) over a timespan covering a Grand Maximum immediately followed by a Grand Minimum. The bottom panel shows the corresponding time-latitude diagram for the toroidal magnetic component at mid-depth in the convection zone. As in the Bushby (2006) model just considered, at Prandtl number $Pm \simeq 1$ this self-excited dynamo settles into a fixed-amplitude cycle (see Fig. 5.7), but for Pm significantly below unity develops a modulation of the cycle amplitude on timescales much longer than the cycle period, with ubiquitous modulation of the solution parity. Here the solution is in a symmetric (quadrupolar-like) state across the high-amplitude phase and subsequent decrease into a very low amplitude, Grand Minimum-like regime, but then re-emerges in an antisymmetric, dipole-like configuration. Similar parity modulation across Grand Minima has been observed in other non-kinematic models of varying levels of complexity (see, e.g., Tobias, 1997; Beer et al., 1998; Sokoloff and Nesme-Ribes, 1994). In this model the mod-

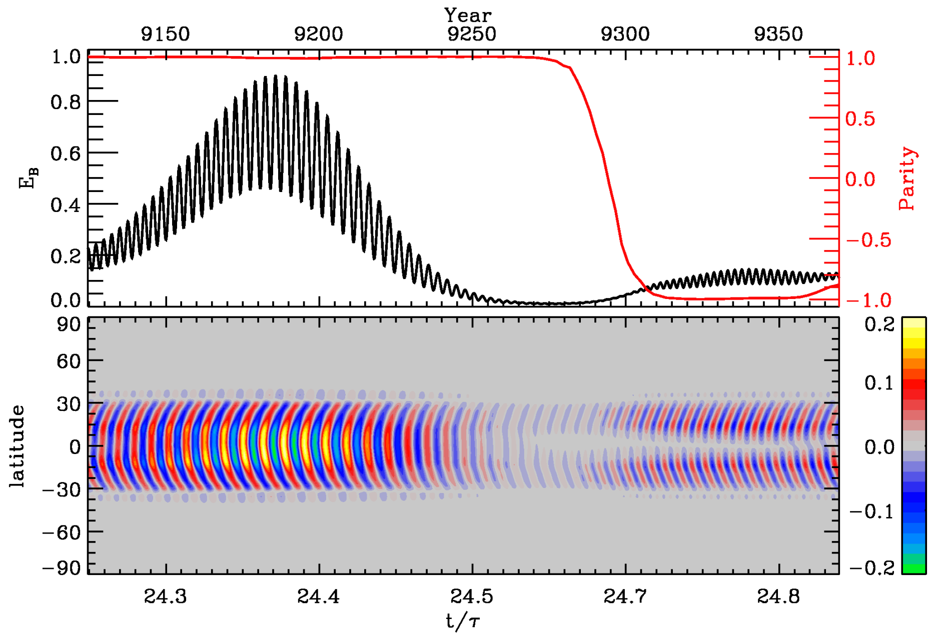

Figure 7.11 Parity modulation in a non-kinematic 2D axisymmetric $\alpha^2\Omega$ mean-field model. This is a low Prandtl number, supercritical solution ($\mathrm{Pm} = 10^{-2}$, $D = 5.25 \times 10^5$) exhibiting chaotic modulation (cf. Fig. 7.10D). {fig:nkin2}

ulation period is found to increase with decreasing Pm, the ratio scaling approximately as Pm^{-1}.

Figure 7.12 shows a time series of magnetic energy for the same solution, but now over a $\sim 10^4$ yr time span, in which the primary cycle has been removed so that only the modulation amplitude remains. Threshold values have been set to identify Grand Minima (blue) and Maxima (red), with values such that the percent time spent in Grand Minima and Maxima is approximately the same as inferred from the radioisotope record. Although not particularly obvious on Fig. 7.12, the inter-event waiting time distributions for Grand Minima and Maxima are both well approximated by exponentials, even though the modulation is here entirely deterministic, i.e., characterized by infinite “memory”.

As noted in 5.1.5, the dynamo-generated magnetic field impacts differential rotation not just through the large-scale Lorentz force, but also through the modulation of hydrodynamical forcing of differential rotation (see Fig. 5.3). In the mean-field context, the magnetically-mediated reduction of Reynolds stresses, otherwise known as Λ-quenching (see ?Kitchatinov et al., 1994,

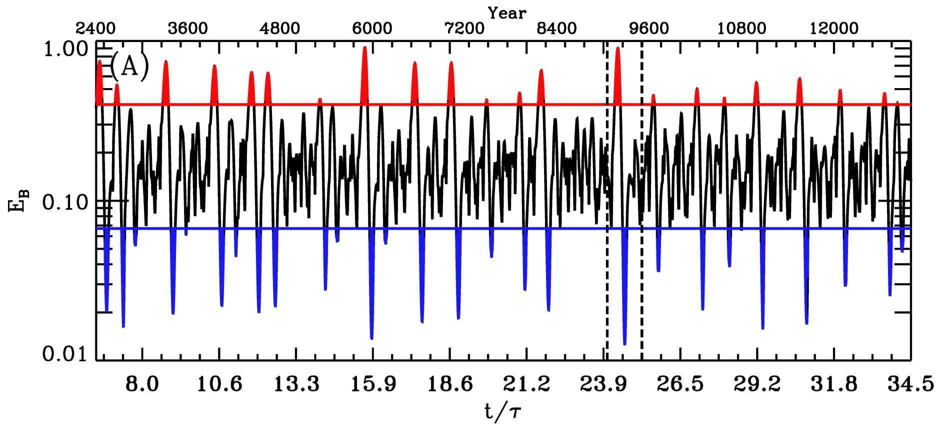

Figure 7.12 Modulation envelope for the cycle amplitude over a 10^4 yr time span in the non-kinematic $\alpha^2\Omega$ mean-field solution of Figure 7.11. Compare to Figs. 7.2, 7.5, 7.6 (bottom), and 7.9.

{fig:nkin3}

also §5.3.5 herein). Küker et al. (1999) have investigated the production of strong amplitude modulation and Grand Minima via this mechanism. If Λ-quenching is strong and dominant over other amplitude-limiting mechanisms, quasiperiodically-recurring Grand Minima are produced in the low (10^{-1}) Prandtl number regime. Entry into and recovery from Grand Minima is gradual, and in their model is accompanied by a reduction of the cycle period by factors ranging from 2 to 4. Lowering the Prandtl number to 10^{-2} yields even more extreme variations, with Grand Minima becoming very rare events.

For other examples of extreme cycle amplitude modulation through nonlinear magnetic backreaction on large-scale flows in a self-excited dynamo, see also Brooke et al. (1998); Pipin (1999); Kitchatinov et al. (1999); Brooke et al. (2002); Phillips et al. (2002).

7.3.5 Global MHD simulations

{ssec:MHDintermi

Global magnetohydrodynamical simulations of turbulent thermally-driven convection and dynamo action (see §5.1) in principle incorporate many of the mechanisms and interplays of mechanisms that can lead to extreme amplitude modulation and/or intermittency. In particular, nonlinear backreaction on flows and a strongly fluctuating turbulent electromotive force are both present, and are captured in a dynamically consistent manner at all spatial and temporal resolved by the simulations.

Figure 7.13 A Grand Minimum in the ASH K3S global MHD simulation of Augustson et al. (2015). The top panel is a time-latitude diagram of the zonally-averaged toroidal magnetic component at $/R = 0.92$, and the bottom panel shows the corresponding time series of power in even (red) and odd (green) axisymmetric ($m = 0$) spherical harmonics modes of the radial field decomposition at $r/R = 0.75$. The vertical dashed line indicate the entry and exit from the Grand Minimum. Figure generated from numerical data kindly provided by K. Augustson. {fig:K3S}

Figure 7.13 shows a segment of a simulation run from the global MHD simulation discussed in Augustson et al. (2015). This is a high-resolution MHD simulation using the ASH code (REFs) with slope-limited diffusion, going under the code name K3S. This low Rossby number simulation operates at three times the solar rotation rate, and generates a solar-like differential rotation profile as well as a regular large-scale magnetic cycle with full magnetic period of 6.2yr and dipole-like equatorial parity. The large-scale magnetic fields accumulates at the base of the domain and develops unipolar large-scale polar caps, as well two equipartition-strength wreath-like twisted toroidal flux systems at mid-latitudes, which migrate equatorward in the course of each half-cycle. Large magnetically-mediated modulation of differential rotation develop in the course of the magnetic cycle, with the mid-latitude large-scale shear reduced by as much as 60% at cycle peak. This deterministic modulation of differential rotation is found to play a key role in the process of magnetic polarity reversal (on this see also Strugarek et al., 2017).

The K3S simulation also produced a Grand Minimum-like event, lasting some 5 half-cycles, and during which the magnetic energy drops by a factor of two. The top panel of Figure 7.13 shows a time-latitude diagram of the toroidal magnetic component at depth $r/R = 0.92$. The disruption of the cycle at low latitudes between $t = 34$ and $50\,\mathrm{yr}$ is quite striking. Note also how the high latitude large-scale fields of the polar caps continues to oscillate even though it fails to reverse polarity throughout this time period.

The disruption of the basic cycle is associated with the excitation of modes of even equatorial parity, with concommitant decrease of odd-parity modes. This is shown on the bottom panel of Fig. 7.13, displaying time series of magnetic energy associated with axisymmetric ($m = 0$) modes of even (red) and odd (green) parity. Theses time series are constructed from the radial magnetic field component at depth $r/R = 0.75$. The switch from dominant odd to even parity is quite swift at $t \simeq 33\,\mathrm{yr}$, with recovery to odd parity taking place more gradually across the Grand Minimum. The detailed analysis of this event carried out by Augustson et al. (2015) reveals that the entry and exit from the Grand Minimum are coincident with the appearance of significant power in the non-axisymmetric ($m \neq 0$) modes, but (for this single Grand Minimum) the most striking precursor if the sudden rise of power in the axisymmetric even modes in the cycle just prior to onset.

The K3S simulation of Augustson et al. (2015) just discussed arguably offers, at this writing, the cleanest analog of a Grand Minimum occuring in a global MHD simulation. Other similar simulations do offer example of other potentially relevant mechanisms for disrupting magnetic cycles developing therein. Figure 7.14, taken from Lawson et al. (2015), depicts the apparent disappearance of the large-scale magnetic cycle in a EULAG-MHD simulation akin to the "millenium simulation" discussed in §5.1. The top time-latitude diagram shows the spatiotemporel evolution of the zonally-averaged toroidal magnetic component at the interface between the convectively unstable fluid and the underlying stably stratified fluid layer present in this simulation. A regular cycle showing good hemispheric synchrony and antisymmetric parity develops after about 100 yr of simulate time, and perdures for another 250 yr until the Southern hemsphere fails to reverse its polarity. The subsequent two (half-)cycles are then parity symmetric, but at $t \simeq 500\,\mathrm{yr}$ the Northern hemisphere shuts off, followed half a half-cycle later by the Southern hemisphere.

In fact, as shown on the bottom panel of Fig. 7.14, the large-scale magnetic

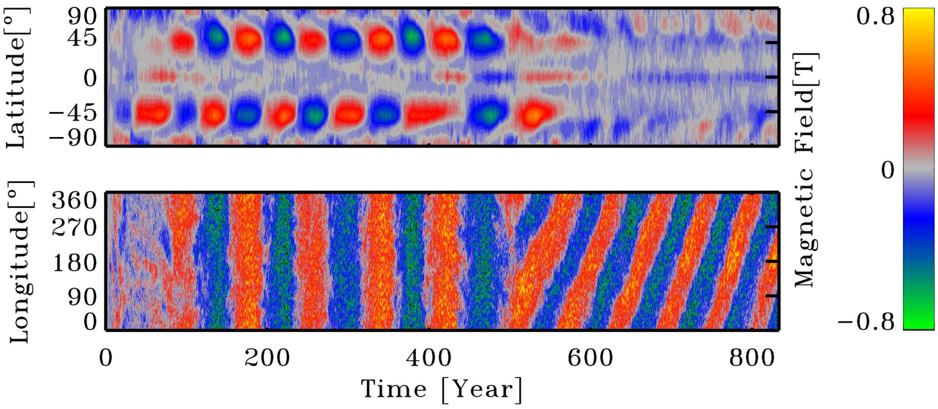

Figure 7.14 Dynamo mode transitions in a EULAG-MHD global simulation of convection and dynamo action, akin to the Passos and Charbonneau (2014) simulation discussed in §5.1. The top panel is a time-latitude diagram of the zonally averaged toroidal magnetic field at the base of the convecting layers ($r/R = 0.71$), while the bottom panel displays a time-longitude diagram of the (unaveraged) toroidal magnetic component extracted at the same depth and latitude 45° North. The apparent disappearance of the large-scale magnetic cycle at $t \simeq 500\,$yr (top panel) is in fact due to the large-scale field transiting to a non-axisymmetric ($m = 1$) "tilted dipole" configuration, still undergoing regular polarity reversals on a multi-decadal timescale (see text). Reproduced from Lawson et al. (2015) (Figure 14). {fig:mhd70}

cycle perdures beyond through the end of this simulation, with roughly the same peak magnetic field strength and slightly reduced cycle period. What is plotted here is now a time-*longitude* diagram extracted at the same depth as the top panel and latitude 45° in the Northern hemisphere. It reveals that at $t \simeq 500\,$yr, what was up to then a cycling axisymmetric large-scale magnetic field (no variation with longitude on global scales) transits abruptly to a non-axisymmetric configuration, which turns out to be well approximated by a dipole strongly tilted with respect to the rotation (symmetry) axis. The analysis of Lawson et al. (2015) suggests that this transition may be triggered by the development of a magnetoshear instability in the upper reaches of the stable fluid layer (on this see also Miesch, 2007, as well as Gilman et al. 2007, and references therein).

The spherical wedge MHD simulation of Käpylä et al. (2016) illustrates yet another potentially relevant mechanism, namely the "destructive interference" between no less than three spatially segregated dynamo modes developing in their simulation (on co-existing dynamo modes in global MHD simulations see also Beaudoin et al., 2016).

7.3.6 All together now

revealed an abundance of riches;

stochatic fluctutions in dynamos near-criticlity

interference between different dynmo modes , be they globa modes ofdifferent parity or spatially segrgated modes

nonlinear modulation of large-scale flows in supercriticall regime

no sunspots, and this no BL mechanism, in global MHD sims

backreaction on flows very simplistic in most mean-field and mean-field-like solar cycle models; paticularly true for modulation of Cm in FTD, almost always forced kinemtically

7.4 Can long-term variability be predicted ? {sec:GMpredict}

Predicting Gmin and Gmax: The climate and space climate issue (next chapter)

Amplitude modulation: deterministic, long-term "memory" ref Fig. 7.10

Stochastically-driven intermittency: fundamentally unpreeictable, but precursors might exist for onset of GMim, depending on physical nature of transition between ynamical dstates

Many Gmin mechanisms described in foregoing sections, relying on distinct underlying "basic" dynamo models and distinct mechanism for amplitude variations. Nonetheless some common precursor patterns emerge

chiefly: large hemispheric asymetry in cycle preceding onset (point to Figs) reflecting parity modulation, or more generally, interaction of modes with distinct symmetries

Most GM scenarios discussed above display gradual recovery to "normal" cyclic behavior; but not so for onset therein lies perhaps a potentially useful discriminant

7.5 Summary

- wide variety of possible scenarios to push a solar/stellar dynamo in and out of quiescent epoch of strongly reduced activity
- purely deterministic nolinear modulation tends to generate periodically or quasi-periodically recurring Grand Minima, often of similar duration.

- scenarios including stochastic mechanisms tend to produce aperiodically recurring GM with a wide distribution of durations.
- dynamo model with lower operating threshold on field strength need a secondary dynamo to restart and exit GM
- some scenarios exhibit a precursor signal to the onset of grand minima (high cycle amplitude, pronounced GO signal, strong hemispheric asymetry).